17th Brazilian Congress of Thermal Sciences and Engineering
November 25th-28th, 2018, Águas de Lindóia, SP, Brazil

ENCIT-2018-0020
PREDICTION OF LASER WELD BEAD PROFILE THROUGH AN INVERSE PROBLEM APPROACH

Elisan dos Santos Magalhães
Heat Transfer Laboratory – LabTC Institute of Mechanical Engineering – IEM, Federal University of Itajubá – UNIFEI, Campus Prof. José Rodrigues Seabra Av. BPS, 1303, 37500-903, Itajubá, MG, Brazil.
elisan@unifei.edu.br

Luiz Eduardo dos Santos Paes
Laboratory of Precision Mechanics – LMP, Department of Mechanical Engineering – EMC, Federal University of Santa Catarina – UFSC, Centro Tecnológico, 88040-900, Florianópolis SC, Brazil.
luiz.paes@posgrad.ufsc.br

Milton Pereira
Laboratory of Precision Mechanics – LMP, Department of Mechanical Engineering – EMC, Federal University of Santa Catarina – UFSC, Centro Tecnológico, 88040-900, Florianópolis SC, Brazil.
Milton.pereira@ufsc.br

Sandro Metrevelle Marcondes Lima e Silva
Heat Transfer Laboratory – LabTC Institute of Mechanical Engineering – IEM, Federal University of Itajubá – UNIFEI, Campus Prof. José Rodrigues Seabra Av. BPS, 1303, 37500-903, Itajubá, MG, Brazil.
metrevel@unifei.edu.br

Abstract. *The heat flux inverse analysis is significantly affected by the heat flux distribution in laser welding simulation. This work proposed a different approach for the heat distribution which predicts the temperature and the weld bead in laser welding. The influence of the heat flux distribution in an inverse heat conduction problem applied on laser welding simulation is studied by comparing different heat distribution models. An inverse heat conduction algorithm based on three-dimensional (3D) heat diffusion equation and the enthalpy function to model the phase change problem are used to estimate the heat flux under different heat distributions. The Time Travelling Regularization is applied with the Golden Section method to estimate the heat flux in the studied cases. The proposed cubic root and square root of the volumetric heat distribution presented a good agreement between the weld profile and the experimental temperatures. The heat rate estimation proves to be dependent on the heat distribution. The proposed methodology is an alternative to predict the weld bead profile and the thermal efficiency in low penetration laser welding.*

Keywords: *Laser welding, Time Travelling Regularization, Inverse problems, Thermal efficiency, Heat flux*.

1. INTRODUCTION

Welding is an important process for the assembly stage in many industries. Inadequate parameters can induce joint defects, which affect integrity of the structure and hinder its application. To optimize these parameters, the empirical approach is usually preferred. However, this involves numerous experimental trials, intended to investigate the influence of each variable involved. Considering the recurrent demand for better productivity and quality, the laser based welding processes have gained higher relevance relative to arc processes. However, this limits the experimentation efforts due to the high cost involved in equipment and consumables, in addition to the need for specialists to operate the systems and the highly restrictive safety requirements. Besides that, experimental procedure is time-consuming. (Ayoola et al. (2017) suggested minimizing these disadvantages through the replacement of usual adopted variables such as laser power and welding speed, by others based on spatial and temporal energy, as power density, interaction time and energy density. Thus, the same choice of parameters can be used for many problems and not only for specific ones. However, it still requires a considerable number of experiments to reach a reliable optimization.

Recently, heat transfer mathematical models have been used to predict the resulting weld geometry as a function of the input process variables. For example, Hadi (2012) applied analytical equations to determine the behavior trends in temperature distribution during laser remelting process. These equations were useful to determine optimal parameters as well as to perform intelligent control. However, the majority of these methodologies considers simplified hypothesis such as infinite workpiece (Mackwood and Crafer, 2005). Although many authors continuously study these

methodologies (Franco et al., 2014; Heller et al., 2017; Volpp, 2017; Volpp and Vollertsen, 2015), the solutions are found mainly for simple conditions.

Complex joint geometries and the three-dimensional nature of the problem lead to the preference for numerical models over others. Ai et al. (2017) demonstrated the feasibility of the numerical approach to predict laser welding results. This is also used to solve the multiphysics phenomena, which correlate heat transfer and solid mechanics differential equations numerically (Ahn et al., 2017; Kouadri-Henni et al., 2017; Liu et al., 2017; Yilbas et al., 2010). From these models, metallurgical information such as phase formation and grain refining can be extracted, as well as those related to mechanical behavior, due to the dependence of resultant strength on microstructure. One way to obtain this information is through the use of Inverse Problems (Gonalves et al., 2010). The Inverse Problems are used to determine the casual factor from the observed effects. Usually in welding, the temperature data are collected and used as an observed effect. In heat transfers studies applied to welding process, the casual factor may be reported by the heat flux, thermal properties, and heat transfer coefficients. For instance, Magalhães et al. (2016) proposed an Inverse methodology to estimate the heat flux for a Gas Tungsten Arc welding process. In their work, the authors proposed a combination of the temperature moving sensor technique and the Time Travelling Regularization. This new technique allowed the thermal efficiency curve determination. This cited work concentrated on the voltage arc process GTAW. There is currently not much information available covering the use of this approach of the focused heat sources, as the light beam originated from a laser. It must be emphasized that laser heat source shows distinct characteristics when compared to arc processes, which require the development of an appropriate model for this approach.

The joining of materials that are susceptible to undesirable metallurgical transformations, as in structures where deformation and residual stresses are not tolerated, usually leads to a coherent light beam as the process heat source, the laser. The equipment has a set of optical components such as optical fibers, mirrors and lenses, able to focus the energy, and as a result promote localized fusion over the surface of the processed material. Besides the benefits regarding the narrow Heat Affected Zone (HAZ), which is a typical feature of this process, it is important to mention the significant raise in productivity compared to arc voltage processes, as well as the feasibility to weld in difficult access areas, as it does not require torches or tools near the workpiece (Jenney and O'Brien, 1991; Poprawe, 2011).

Considering the variation of parameters such as energy density and welding speed, the user can choose between two possible operation modes. The keyhole mode, known as deep penetration mode, dependent on metallic vaporization (Ebrahimi et al., 2016) and consequent gas ionization on the incidence laser point over the workpiece leading to plasma formation. Then, the weld pool surface breaks allowing direct radiation transfer from laser beam to the solid-liquid interface, resulting in a deep cavity. This reaches the maximum height when the laser energy is no longer sufficient to melt the rear material, causing a stabilization of the keyhole regime after the forces are balanced. As the laser beam progresses over the workpiece surface, a propagation front is induced and the fused metal fills the initial cavity, originating beads with penetration/width ration around 10:1(Poprawe, 2011). Even though this laser processing mode is suggested for joining applications, the metallic vaporization hinders its control and stability, which increases the defect susceptibility. Therefore, in critical circumstances, the conduction mode is preferred (Ai et al., 2016; Eriksson et al., 2014).

In conduction welding mode, metallic vaporization is not expressive. Then, the melting pool has a much more stable behavior, with a lower defect incidence (Ayoola et al., 2017; Meco et al., 2013; Sanchez-Amaya et al., 2009). The energy emitted by the laser is partially absorbed by the material, and, conduction heat transfer governs this situation (Ion, 2005). Thus, contrary to keyhole mode, the weld bead exhibits a wider width and a shallow penetration, similarly to arc welding beads. Comparing these results to those obtained through conventional welding, the main gain is due to higher processing speeds and lower deformation levels in the structure. This paper concentrates on conduction welding mode behavior.

In order to determine the best approach for the heat flux distribution in a laser welding process, 4 (four) volumetric heat flux distributions for the laser welding process are proposed. The volumetric heat flux distributions are compared to the classical model proposed by Goldak and Akhlaghi (2005). The best approach is expected to predict the experimental temperatures and the transversal weld bead profile. The heat flux was estimated through the methodology proposed by Magalhães et al. (Magalhães et al., 2016). In this methodology, the inverse methodology Time Traveling Regularization (TTR) and the temperature moving sensor technique are applied together to determine the average thermal efficiency of the analyzed cases.

2. METHODOLOGY

2.1 Termal model

This work considered a non-linear three-dimensional heat transfer model with phase change modeled by the enthalpy equation and temperature-dependent thermal properties. Those equations have been solved through the Finite Difference method. Details of the software theoretical development and boundary conditions have been reported in Magalhaes et al. (2017).

2.2 Heat flux distribution

In laser welding, the weld is done through the heat delivered by the laser welding head. In welding simulation, this heat can be distributed according to some mathematical models. The heat distribution can be analyzed by two and three-dimensional approaches. Usually, the two-dimensional (2D) heat distribution can be obtained in two ways: a linear or Gaussian. The linear heat flux distribution over a circular area can be written as:

$$q''(x,y,t)=\frac{Q(t)}{\pi R^2}\left((x-u\,t)^2+y^2\right) \tag{1}$$

where *q*" is the heat flux, *Q* is the gross heat rate, *R* is the weld radius and *u* is the welding speed. The Gaussian heat distribution is defined by:

$$q''(x,y,t)=\frac{Q(t)}{\pi R^2}e^{-3\frac{(x-ut)^2}{r^2}}e^{-3\frac{y^2}{r^2}} \tag{2}$$

The three-dimensional heat distribution applied in this work is based on a conical distribution of power density. This approach was suggested by Goldak and Akhlaghi (2005) for the laser welding process. It has a radial Gaussian distribution and an axial linear distribution. Figure 1 presents the distribution scheme, where *h* is the welding penetration:

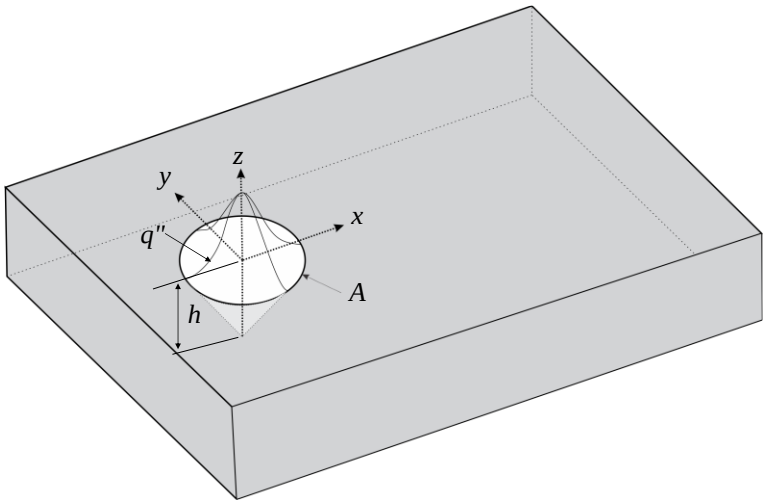

Figure 1. Conical heat flux distribution in the laser welding process.

A radial Gaussian distribution and a rational function for the heat distribution are proposed in this work. The linear heat flux distribution simulates the barrier effect that the laser beam is subject while it penetrates the sample. Although this model can predict the width and penetration size of the weld bead, it cannot predict its shape. The proposed model considers that the heat flux is distributed following a polynomial function distribution. Four approaches are considered. The two first approaches consider the heat distribution as a square and cubic function. The two others consider the heat flux distribution as a square and cubic root. These approaches consider the heat flux distribution higher on the surface than when it approaches the penetration coordinate *h*. Figure 2 presents the difference between the heat flux distributions in coordinate *z* for the linear and all the cases proposed. Equations (3) to (7) present the five analyzed volumetric heat distribution cases. The heat distributions for the scheme presented in Fig. 1 can be expressed as:

A01: $$\dot{q}(x,y,z,t)=\frac{4Q(t)}{\pi R^2 h}e^{-3\frac{(x-ut)^2}{r^2}}e^{-3\frac{y^2}{r^2}}\left(\frac{1}{h}-\frac{z^3}{h^3}\right) \tag{3}$$

A02: $$\dot{q}(x,y,z,t)=\frac{3Q(t)}{\pi R^2 h}e^{-3\frac{(x-ut)^2}{r^2}}e^{-3\frac{y^2}{r^2}}\left(\frac{1}{h}-\frac{z^2}{h^2}\right) \tag{4}$$

A03: $$\dot{q}(x,y,z,t) = \frac{2Q(t)}{\pi R^2 h} e^{-3\frac{(x-ut)^2}{r^2}} e^{-3\frac{y^2}{r^2}} \left(\frac{1}{h} - \frac{z}{h} \right) \quad (5)$$

A04: $$\dot{q}(x,y,z,t) = \frac{3Q(t)}{2\pi R^2 h} e^{-3\frac{(x-ut)^2}{r^2}} e^{-3\frac{y^2}{r^2}} \left(\frac{1}{h} - \frac{z^{1/2}}{h^{1/2}} \right) \quad (6)$$

A05: $$\dot{q}(x,y,z,t) = \frac{4Q(t)}{3\pi R^2 h} e^{-3\frac{(x-ut)^2}{r^2}} e^{-3\frac{y^2}{r^2}} \left(\frac{1}{h} - \frac{z^{1/3}}{h^{1/3}} \right) \quad (7)$$

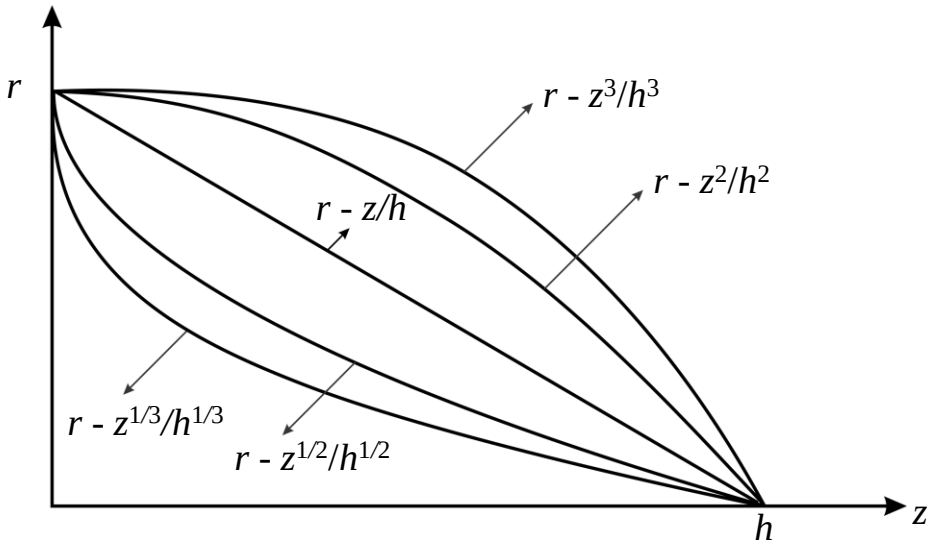

Figure 2. Heat distribution in axis *z* considering linear, square and cubic functions, and square and cubic root functions.

2.3 Inverse problem

The inverse methodology presented in this work is based on an Inverse Heat Conduction Problem (IHCP). The inverse method Time Travelling Regularization was applied on the Golden Section minimization method (Vanderplaats, 2005) to minimize the noise interference and the Settling Time (Shirtliffe, 1974). The temperature moving sensor methodology proposed by Magalhães et al. (2016) allows the thermal efficiency estimation in welding as a time-dependent function.

This method requires an Objective Function to be minimized written as:

$$F_{obj}^{j} = \sum_{i=j}^{j+r} \left(Y^{j+r} - T^{j+r} \right)^2 \quad (4)$$

where F_{obj} is the Objective Function, Y is the experimental temperature, T is the numerical temperature, j is the counter for the time step and r is the number of future time steps.

3. MATERIALS, EXPERIMENTS AND SIMULATIONS

3.1 Materials and methods

The experiments were performed with a fiber laser power source IPG-YLS 10000 of maximum power output of 10 kW, attached to an optical fiber and a Precitec YW52 processing head. The beam was adjusted to its focal distance, which resulted in 880 μm diameter over the sample, with Gaussian distribution. To ensure operation in the conduction mode, the chosen parameters were 3 kW of power and 3 m/min of welding speed. This input power was chosen in order to minimize the keyhole mode in the laser welding process. Three experiments were conducted aiming to assure the repeatability of the measured temperatures and welding shape.

For temperature acquisition, a National Instruments USB 6218 board with 32 inputs, 16 bits and 250 kb/s was selected. The acquisition rate was 0.1 s (10 Hz). Type K thermocouples were preferred due to their capability of reaching temperatures up to 1370 °C. The thermocouples were fixed through capacitive discharge. Figure 3a presents the experimental apparatus used in the experiment. 9.5 mm x 31 mm x 207 mm samples were made of SAE 1020 steel. Each weld bead had a length of 45.0 mm. Figure 3b presents the thermocouple locations on the SAE 1020 steel sample. In Figure 4, the described configuration, including equally fixed thermocouples (Δy = 5.0 ± 0.5 mm and Δx = 1.8 ± 0.2 mm) is presented.

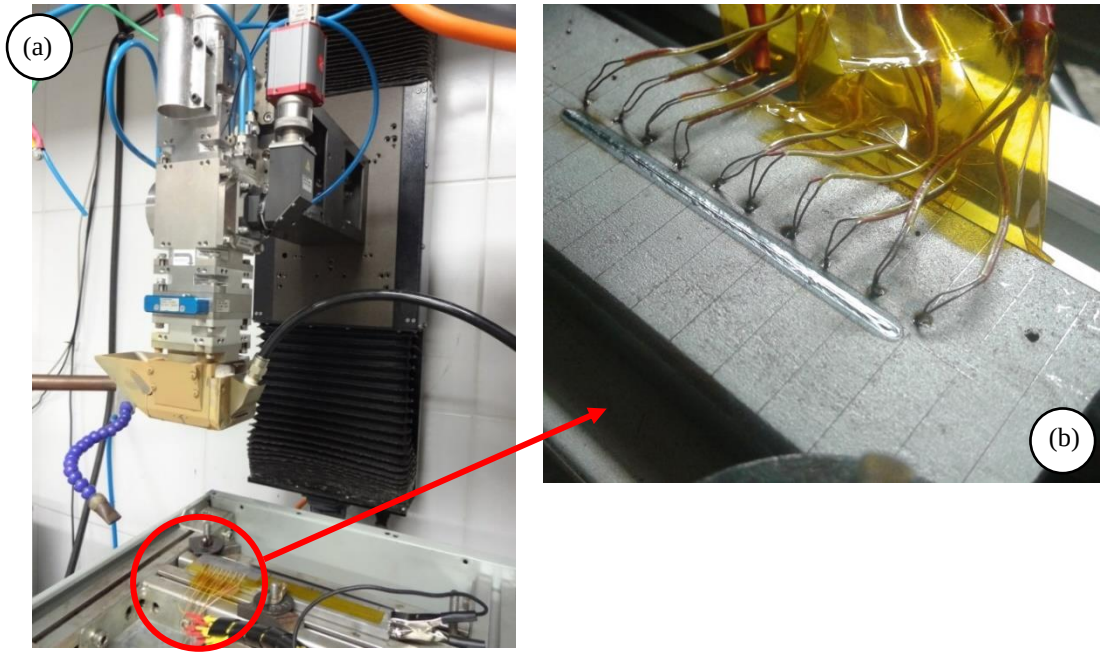

Figure 3. a) Experimental assembly: laser weld head, sample and thermocouples, b) Thermocouple position.

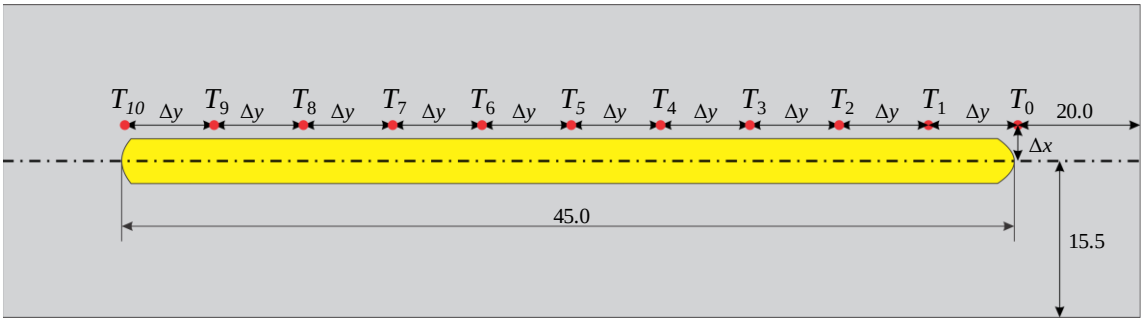

Figure 4. Thermocouple locations and distributions on the SAE 1020 steel.

3.2 Simulations

To simulate the laser welding problem, previously developed software was adapted to consider a volumetric heat distribution. The software theoretical development was reported in Magalhaes et al. (2017). A non-uniform mesh with 1,936,000 volumes was applied to simulate the problem. The mesh size was determined by a mesh convergence test. The thermal properties were obtained from fitting data points of Touloukian et al. (1975). Goldak and Akhlaghi (2005) proposed that the convection in the fusion zone can be approximated by increasing the thermal conductivity when the temperature reaches the melting point. This approach was adapted in this work. The thermal conductivity λ [W/mK] was increased twice when the melting point was reached. The thermal conductivity and thermal diffusivity α [m²/s] curves are expressed by:

$$\lambda(T) = \begin{cases} -2.904\times10^{-2}T + 55.94 & for \;\; T < 1425°C \\ 111.88 & for \;\; T \geq 1425°C \end{cases} \tag{5}$$

$$\alpha(T) = \begin{cases} -1.162\times10^{-8}T + 1.308\times10^{-5} & for \;\; T < 700°C \\ 4.946\times10^{-6} & for \;\; T \geq 700°C \end{cases} \tag{6}$$

4. RESULTS AND DISCUSSION

The analyzed volumetric heat distributions are studied under two aspects. A shape analysis is proposed to select the best heat distribution approach for the inverse estimation. The ideal model should predict both the laser weld shape and the temperature at experimentally measured points.

4.1 Weld shape analysis

In order to compare the transversal weld bead profile, a microstructural analysis was made. Figure 5 exhibits the resulting transversal weld bead profile, with the correspondent width and penetration dimensions. Three regions can be delimitated: the Fusion Zone (FZ), where temperature exceeded the fusion point, and therefore, dendritic solidification was predominant; the Heat Affected Zone (HAZ), where fusion temperature was not reached, but significant microstructure changes happened; and finally, the Base Metal (BM), where the microstructure was not affected due to thermal cycles.

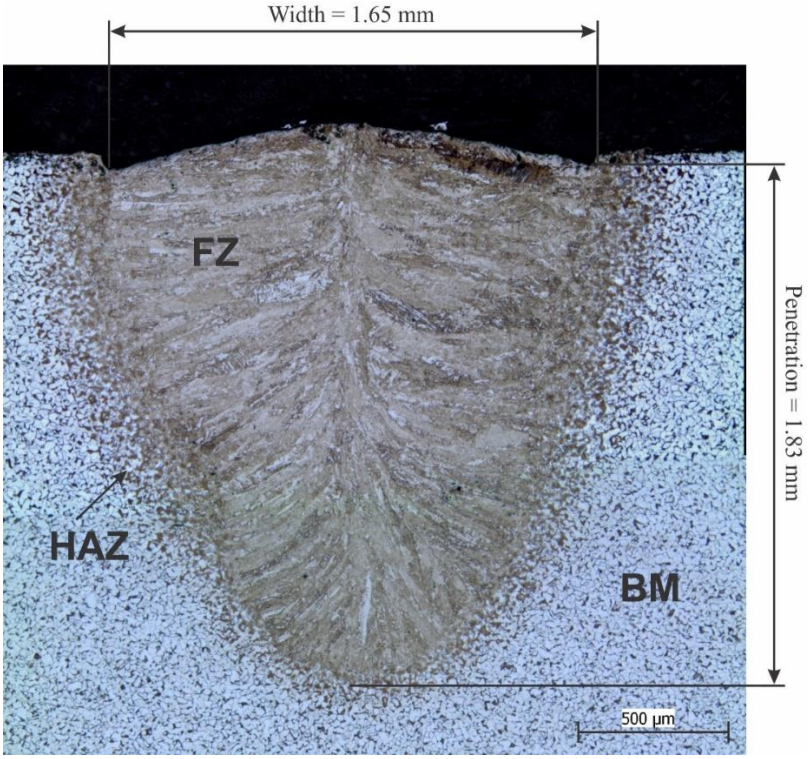

Figure 5. Transversal weld bead profile with its corresponding width and penetration dimensions.

A 2D Gaussian heat flux distribution was used to analyze the width and penetration of the weld bead profile. The mass fraction transversal profile may be analyzed in Fig. 6 where the predicted width and penetration for a 2D heat flux distribution are presented. It may be noticed that although the width is similar to the experimental results, the penetration is significantly different. This mass fraction distribution was expected. In fact, 2D heat flux models cannot predict the weld bead profile, since it considers that all the heat is delivered on the surface. The laser welding process has a particular characteristic, in fact the laser beam penetrates the sample, and therefore it requires a volumetric heat distribution.

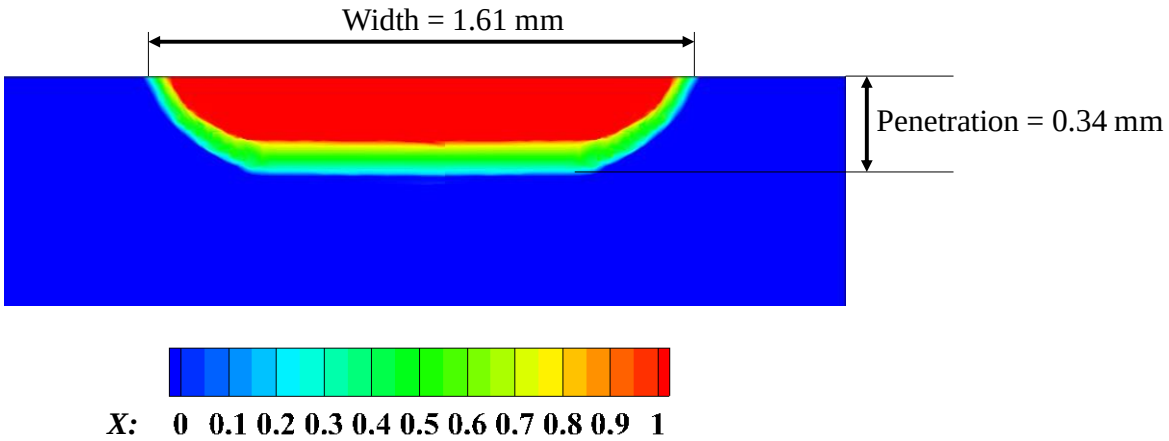

Figure 6. Mass fraction (X) for a 2D Gaussian heat flux distribution.

The 3D volumetric heat distribution cases presented better results when compared to the 2D models. Table 1 presents the width and penetration values obtained for the five analyzed cases. It may be seen in Tab. 1 that the values obtained numerically are in good agreement with the experimental values. However, the main difference among them was the weld shape. Figure 7 presents the weld shape for the analyzed cases. In Figure 7, cases A01 and A02 presented a welding profile different from the experimental case. Due to their mathematical configuration, the welding profile in the weld face is linear and it changes to round in its root. A03 is a classical linear case which better approached the welding profile than the cases A01 and A02. However, the linear distribution made a plane in the weld root of the welding profile, which do not represent the experimental configuration. Case A04 presented a linear welding profile followed by a rounded curve in the weld root. Case A05 presented a better welding profile when compared to the experimental one (Fig. 5). Cases A04 and A05 presented better results due to their mathematical approach which simulates the real process better. Indeed, the laser beam did not penetrate uniformly on the first layers of the sample as proposed by models A01 and A02, and it does not have a linear drop as the classical method A03. Therefore, the proposed cases A04 and A05 better approach the physical problem.

Table 1. Numerical values for width and penetration for the five analyzed cases.

Case	Width [mm]	Penetration [mm]
Experimental	1.65	1.83
A01	1.59	1.89
A02	1.68	1.88
A03	1.63	1.78
A04	1.64	1.81
A05	1.65	1.80

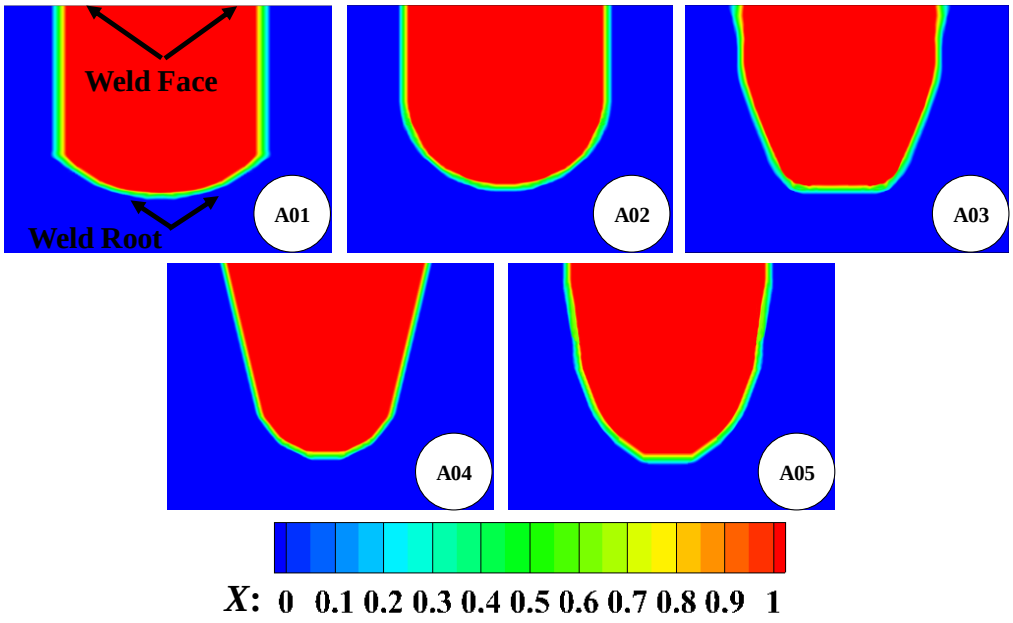

Figure 7. Welding profile represented by the mass fraction (X) for the five analyzed cases.

Figure 8 presents the overlay of the temperature field of case A05 and the microstructural analysis (Fig. 5). From this analysis, it is possible to obtain the temperature that could have a thermal effect on the properties of the material. For instance, in this material, the FZ comprehends the region with temperature above 1450°C (the fusion temperature); the HAZ has temperature between 850°C and 1450°C; and the BM has temperatures under 850°C.

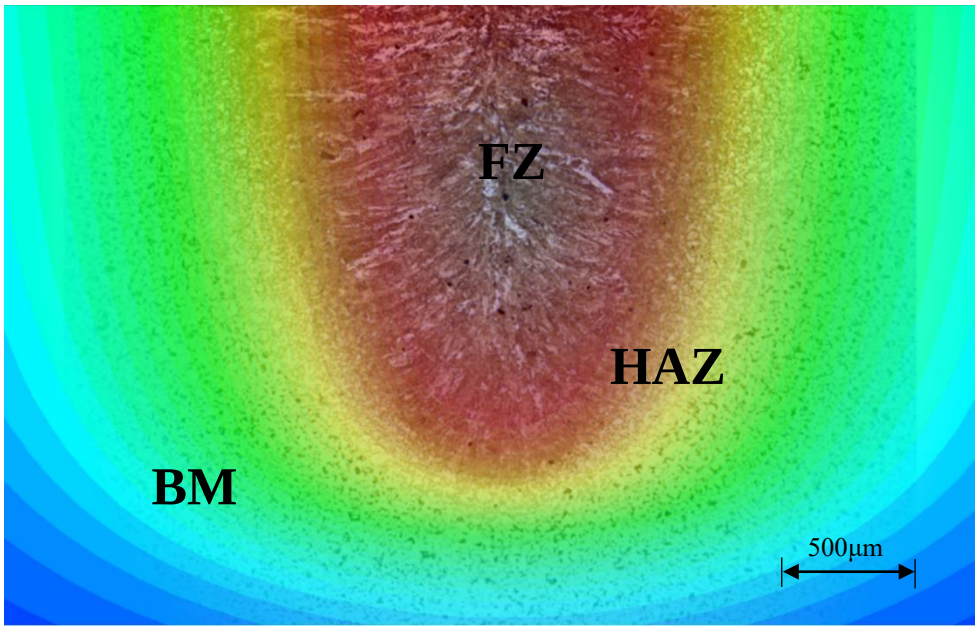

Figure 8. Temperature field for Case A05 combined with weld micrography (Fig. 5).

4.2 Thermal analysis

A comparison between the experimental temperature values of thermocouple T_1 (Fig. 4) and the numerical temperatures is presented in Fig. 9. The five analyzed cases presented a good agreement between the curves. However, the numerical peak temperature differs for all the cases. Cases A04 and A05 presented the highest peak temperature. This can be explained by the experimental approach; the thermocouples were positioned on the welding surface near the weld bead, thus, a higher heat rate closer to the welding surface provides high temperatures where the thermocouples were positioned. The chosen measurement area is highly sensitive, therefore, the measurement error in the position of

the thermocouple is enough to present this kind of peak temperature difference. It is worth to remember that cases A04 and A05 presented a better weld shape than cases A01, A02 and A03. Cases A01, A02 and A03 presented a good agreement in relation to the experimental curve. However, those models failed to predict the welding shape, therefore, they are not reliable to perform inverse analysis.

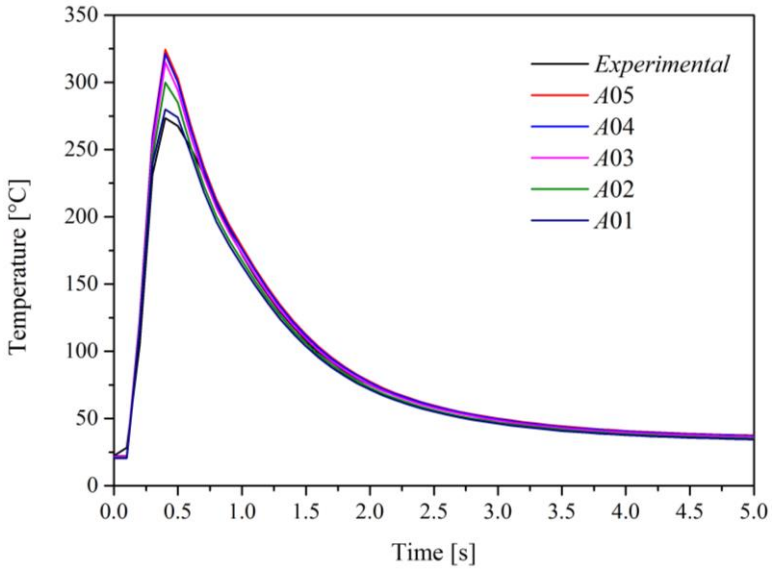

Figure 9. Comparison between the experimental and numerical temperatures for test A01 to A05.

Table 2 presents the average estimated heat rate for the five analyzed cases. The thermal efficiency (η_T) differs significantly for each analyzed case. Cases A01 and A02 presented higher thermal efficiency values than cases A03, A04 and A05. In those cases, the cubic and square function made the heat distribution more uniform along the axis *z*, which decreased the temperature on the surface, providing a better agreement between the experimental and numerical temperatures. Therefore, the thermal efficiency increased due to the lower sensitivity presented in the model. Although the linear case presented a coherent thermal efficiency value, it did not present a good agreement concerning the welding shape. Thus, it may not represent the real value. Cases A04 and A05 presented a good agreement concerning the transversal weld bead profile. As those models have higher sensitivity in relation to the others, the estimated heat rate tends to decrease. Thus, cases A04 and A05 present reliable values for the analyzed laser welding condition.

Table 2. Comparison of the estimated heat rate for the cases analyzed.

Case	**Generated power (W)**	**Estimated heat rate [W]**	**η_T [%]**
A01	2990	2523	84.4
A02	2990	2395	80.1
A03	2990	2254	75.4
A04	2990	2187	73.1
A05	2990	2156	72.1

Figure 10 presents the approximated curve for the temperature moving sensor built from experimental temperatures (Fig. 4). It may be noticed that the temperature is established around 275°C. For further details on the temperature moving sensor, please see Magalhães et al. (Magalhães et al., 2016). The estimated heat rate for the five analyzed conditions is presented in Fig. 11. As presented in Tab. 1, the estimated heat rate is higher for the cases A01, A02 and A03, and it starts to converge for cases A04 and A05.

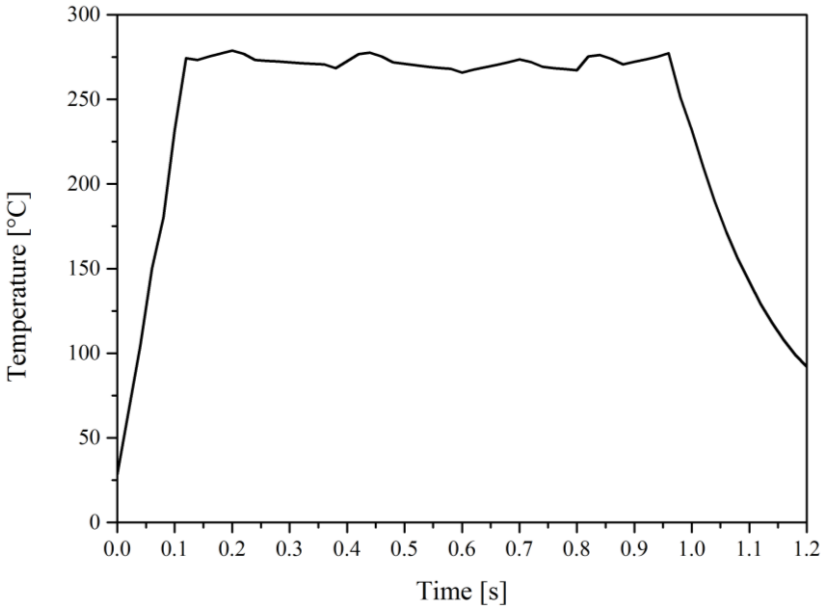

Figure 10. Temperature in the moving sensor.

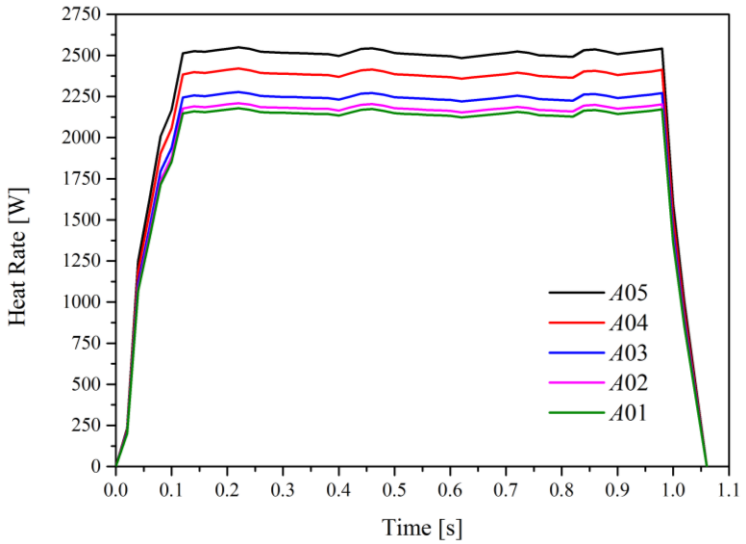

Figure 11. Estimated heat rate for the proposed cases.

Figure 12 presents the heat distribution for case A05. It may be observed that the heat is concentrated together with the laser beam. Due to the welding velocity, the heating diffusion is slower than the heat flux. Thus, this process does not pre-heat the sample as occurs in the traditional welding processes.

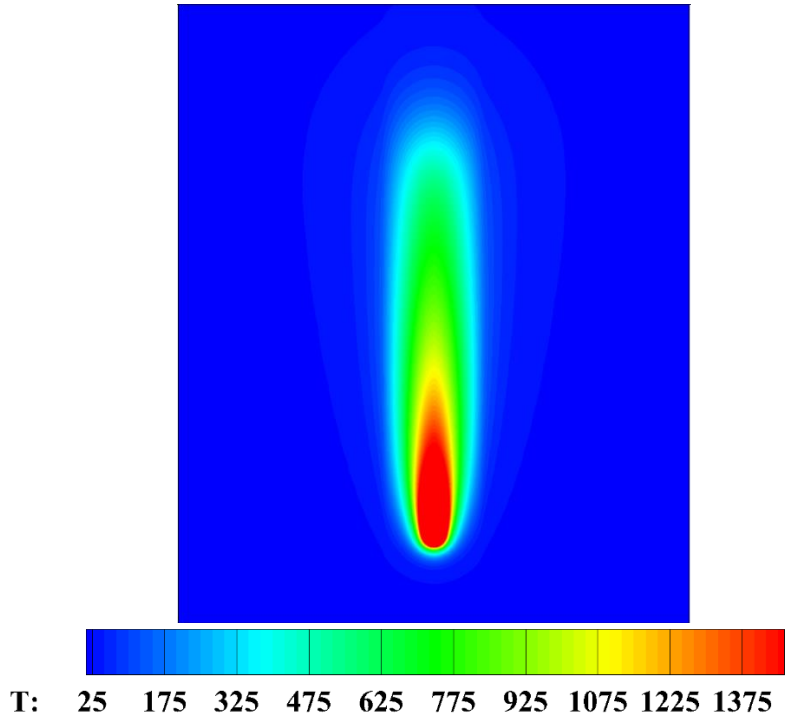

Figure 12. Heat distribution for case A05.

5. CONCLUSIONS

An analysis of the volumetric heat flux distribution in a laser welding process was presented. Four volumetric heat distribution models were proposed and compared with the classical model in Goldak and Akhlaghi (2005). The models based on a square and cubic functions, cases A01 and A02, do not present a good agreement in relation to the experimental weld profile. In addition, those models overload the heat rate estimation due to the sensitivity loss. The classical model presented a better agreement in relation to the experimental weld profile. However, case A03 has not matched the weld profile as cases A04 and A05. Cases A04 and A05 presented good agreement with the weld profile. The heat rate estimation of those models presented more realistic values than cases A01, A02 and A03. The proposed methodology proved to be an alternative tool to predict the weld bead profile and the thermal efficiency in low penetration laser welding.

6. ACKNOWLEDGMENTS

The authors thank CNPq, CAPES and FAPEMIG for their financial support.

7. REFERENCES

Ahn, J., He, E., Chen, L., Wimpory, R.C., Dear, J.P., Davies, C.M., 2017. Prediction and measurement of residual stresses and distortions in fibre laser welded Ti-6Al-4V considering phase transformation. Mater. Des. 115, 441–457. doi:10.1016/j.matdes.2016.11.078

Ai, Y., Jiang, P., Shao, X., Li, P., Wang, C., Mi, G., Geng, S., Liu, Y., Liu, W., 2017. The prediction of the whole weld in fiber laser keyhole welding based on numerical simulation. Appl. Therm. Eng. 113, 980–993. doi:10.1016/j.applthermaleng.2016.11.050

Ai, Y., Jiang, P., Shao, X., Wang, C., Li, P., Mi, G., Liu, Y., Liu, W., 2016. An optimization method for defects reduction in fiber laser keyhole welding. Appl. Phys. A Mater. Sci. Process. 122, 1–14. doi:10.1007/s00339-015-9555-8

Ayoola, W.A., Suder, W.J., Williams, S.W., 2017. Parameters controlling weld bead profile in conduction laser welding. J. Mater. Process. Technol. 249, 522–530. doi:10.1016/j.jmatprotec.2017.06.026

Ebrahimi, A.N., Arab, N.B.M., Gollo, M.H., 2016. Thermal analysis of laser beam welding of nickel-based super alloy

Inconel 625 to AISI 316L, using Gaussian optics theory in keyhole. J. Brazilian Soc. Mech. Sci. Eng. 38, 1199–1206. doi:10.1007/s40430-015-0422-5

Eriksson, I., Powell, J., Kaplan, A.F.H., 2014. Surface tension generated defects in full penetration laser keyhole welding. J. Laser Appl. 26, 12006. doi:10.2351/1.4830175

Franco, A., Romoli, L., Musacchio, A., 2014. Modelling for predicting seam geometry in laser beam welding of stainless steel. Int. J. Therm. Sci. 79, 194–205. doi:10.1016/j.ijthermalsci.2014.01.003

Goldak, J.A., Akhlaghi, M., 2005. Computational welding mechanics, Computational Welding Mechanics. Springer. doi:10.1007/b101137

Gonalves, C.V., Carvalho, S.R., Guimarães, G., Gonçalves, C.V., Carvalho, S.R., Guimarães, G., 2010. Application of optimization techniques and the enthalpy method to solve a 3D-inverse problem during a TIG welding process. Appl. Therm. Eng. 30, 2396–2402. doi:10.1016/j.applthermaleng.2010.06.009

Hadi, I., 2012. Mathematical estimation of melt depth in conduction mode of laser spot remelting process. J. Appl. Phys. 112. doi:10.1063/1.4769868

Heller, K., Kessler, S., Dorsch, F., Berger, P., Graf, T., 2017. Analytical description of the surface temperature for the characterization of laser welding processes. Int. J. Heat Mass Transf. 106, 958–969. doi:10.1016/j.ijheatmasstransfer.2016.10.057

Ion, J.C., 2005. Laser Processing of Engineering Materials: Principles, Procedure and Industrial Application. Laser Process. Eng. Mater. 576. doi:0750660791

Jenney, C.L., O'Brien, A., 1991. Welding handbook, American Welding Society. doi:10.1017/CBO9781107415324.004

Kouadri-Henni, A., Seang, C., Malard, B., Klosek, V., 2017. Residual stresses induced by laser welding process in the case of a dual-phase steel DP600: Simulation and experimental approaches. Mater. Des. 123, 89–102. doi:10.1016/j.matdes.2017.03.022

Liu, S., Kouadri-Henni, A., Gavrus, A., 2017. Numerical simulation and experimental investigation on the residual stresses in a laser beam welded dual phase DP600 steel plate: Thermo-mechanical material plasticity model. Int. J. Mech. Sci. 122, 235–343. doi:10.1016/j.ijmecsci.2017.01.006

Mackwood, A.P., Crafer, R.C., 2005. Thermal modelling of laser welding and related processes: A literature review. Opt. Laser Technol. 37, 99–115. doi:10.1016/j.optlastec.2004.02.017

Magalhães, E.D.S., Lima e Silva, A.L.F. De, Lima e Silva, S.M.M. de, 2016. A THERMAL EFFICIENCY ANALISYS OF GTAW PROCESS IN STAINLESS STEEL, in: 16th Brazilian Congress of Thermal Sciences and Engineering. ABCM, Vitória-Brazil, p. 8.

Magalhaes, E.S., Lima e Silva, A.L.F., Lima e Silva, S.M.M., 2017. A GTA Welding Cooling Rate Analysis on Stainless Steel and Aluminum Using Inverse Problems. Appl. Sci. 7, 122. doi:10.3390/app7020122

Meco, S., Pardal, G., Ganguly, S., Miranda, R.M., Quintino, L., Williams, S., 2013. Overlap conduction laser welding of aluminium to steel. Int. J. Adv. Manuf. Technol. 67, 647–654. doi:10.1007/s00170-012-4512-6

Poprawe, R., 2011. Tailored Light 2. Springer. doi:10.1007/978-3-642-01237-2

S??nchez-Amaya, J.M., Delgado, T., Gonz??lez-Rovira, L., Botana, F.J., 2009. Laser welding of aluminium alloys 5083 and 6082 under conduction regime. Appl. Surf. Sci. 255, 9512–9521. doi:10.1016/j.apsusc.2009.07.081

Shirtliffe, C.J., 1974. Establishing Steady-State Thermal Conditions in Flat Slab Specimens. Heat Transm. Meas. Therm. Insul. Am. Soc. Test. Mater. ASTM STP 5, 13–33.

Touloukian, Y.S., Kirby, R.K., Taylor, R.E., Desai, P.D., 1975. Volume 1 : Thermal conductivity - Metallic elements and alloys, in: Thermophysical Properties of Matter-the TPRC Data Series. p. 1595. doi:10.1007/s13398-014-0173-7.2

Vanderplaats, G.N., 2005. Numerical optimization techniques for engineering design, 4th ed. Vanderplaats Research and Development Inc.,.

Volpp, J., 2017. Keyhole stability during laser welding???Part II: process pores and spatters. Prod. Eng. 11, 9–18. doi:10.1007/s11740-016-0705-4

Volpp, J., Vollertsen, F., 2015. Modeling keyhole oscillations during laser deep penetration welding at different spatial laser intensity distributions. Prod. Eng. 9, 167–178. doi:10.1007/s11740-014-0594-3

Yilbas, B.S., Arif, A.F.M., Abdul Aleem, B.J., 2010. Laser welding of low carbon steel and thermal stress analysis. Opt. Laser Technol. 42, 760–768. doi:10.1016/j.optlastec.2009.11.024

8. RESPONSIBILITY NOTICE

The authors are the only responsible for the printed material included in this paper.